 Cytometry 28:298–304 (1997)

Quantitation of Cell-Matrix Adhesion Using Confocal Image Analysis of Focal Contact Associated Proteins and Interference Reflection Microscopy

Yves Usson,[1]* Alain Guignandon,[2] Norbert Laroche,[2] Marie-Hélène Lafage-Proust,[2] and Laurence Vico[2]

[1]Laboratoire DyOGen, Université Joseph Fourier, Grenoble, France
[2]Laboratoire de Biologie des Tissus Osseux, Université Jean Monnet, Saint-Etienne, France

Received 29 August 1996; Accepted 12 March 1997

We have developed an approach for the quantitation of vinculin, a focal contact associated protein, based on a multimodal confocal microscopy and image analysis. Vinculin spot distribution was imaged in confocal fluorescence microscopy and the corresponding focal contacts were imaged in confocal interference reflection microscopy. These images were analyzed with a SAMBA image cytometer. The image analysis program provided 12 morphometric features describing cellular area, shape, and proportions of vinculin spots as well as six topographical features describing the distribution of vinculin and the relative overlap of vinculin and focal contacts. This approach was applied to the study of rat osteosarcoma cells submitted to mechanical stresses: successions of 2*g* and 0*g* accelerations during a series of parabolic flights. The measured features were assessed by means of correlation analysis and stepwise discriminant analysis. After correlation analysis, only ten parameters were retained. Quantitation of cell morphological parameters indicated that cell area was significantly affected by gravitational stresses as well as vinculin distribution. Cell area was reduced by 50% and vinculin spots were restricted to cell periphery. Cell adhesion measured by IRM decreased significantly in the first part of the flight and remained stable at the end of the flight. These results suggest that cell-matrix adhesion is affected by gravitational stresses. Image analysis provides useful tools to investigate focal adhesion re-organization under different physiological stimuli. Cytometry 28:298–304, 1997. © 1997 Wiley-Liss, Inc.

Key terms: cellular adhesion; osteoblast; microgravity; vinculin; image analysis; confocal microscopy; fluorescence microscopy; reflection microscopy

There is now a large body of evidence that mechanical loading plays a critical role in bone cell function and differentiation (13). However, the precise mechanisms that regulate the transduction of a mechanical signal into a biochemical signal remain unknown. Osteoblasts are more sensitive to a large category of mechanical stresses (i.e., hypergravity, shear stress, hydrostatic pressure) than fibroblasts or endothelial cells (7) and osteosarcoma cells (ROS 17/2.8) are known to be sensitive to mechanical stress (9) or to microgravity (6). While most of the studies focused on mechanical signal transduction in a biochemical message, little is known about the organization of cell adhesion structure, which is one of the mechanotransductors. Previous studies suggested that mechanical stimulation is probably mediated through focal adhesion plaques (18). Vinculin is a cytoskeletal protein that mainly co-localizes to focal adhesions, specialized regions of the cell involved in attachment to the extracellular matrix (19). Vinculin is part of a complex structure that links the actin network to the plasma membrane and contains a focal adhesion targeting sequence (2). A significant proportion of vinculin is organized into a detergent-resistant juxtamembranous structure (focal adhesion plaque) (5,8). Vinculin, when revealed by immunostaining (vinculin containing structures associated with integrins (12,3)) can be found both at cell–cell and cell-matrix adherens junction and near the nuclear envelope. In ROS 17/2.8 (osteosarcoma cell line) we observed that vinculin immunostaining was strongly correlated with close contact areas (all physical contacts between the basal membrane and the substratum), shown by interference reflection microscopy. In ROS the vinculin spots are larger and more clustered than in NIH3T3 and cell–cell staining is present as small

*Correspondence to: Dr. Yves Usson, Laboratoire DyOGen, Institut Albert Bonniot, Université Joseph Fourier, Domaine de la Merci, 38706 La Tronche cedex, France.
E-mail: Yves.Usson@ujf-grenoble.fr

punctuations. Changes in vinculin distribution under mechanical stresses could be appraised by immunostaining (3) but quantitation of these proteins is necessary to better understand rearrangements of focal contacts under mechanical stimulation. Cell adhesion is not entirely dependent on integrin-associated proteins and it is also important to evaluate the physical contacts of the cell with the substratum.

We have developed an approach based on image analysis to measure morphometric and topographic parameters of 1) vinculin immunostaining imaged by confocal scanning laser microscopy (CSLM), and 2) close contacts of cell membrane with the substratum imaged by confocal interference reflection microscopy. This has been applied to cultured cells that were submitted to parabolic flight experiments. The aim was to emphasize the rearrangement of focal adhesion plaques during variation of gravitational stress.

MATERIALS AND METHODS

Cell Cultures

The cells used in this work were rat osteosarcoma cells (ROS 17/2.8) a well-defined osteoblastic cell line. Culture medium was DMEM supplemented with 10% fetal calf serum, 2 mM L-glutamine and 1% penicillin/streptomycin solution. Cells were grown on glass coverslips for 48 hr before immunostaining.

Immunofluorescence Staining

The cells were washed in PBS, fixed, and permeabilized with paraformaldhehyde 4% for 30 min followed by 0.1% Triton X100. Nonspecific binding was blocked by incubation at 37°C in PBS/10% fetal bovine serum. Primary antibody vinculin (diluted 1/100) and FITC conjugate (1/64) were purchased from Sigma, France. The incubations of antibodies were carried out at 37°C for 45 min. Cells were extensively washed in PBS between incubations and mounted in PBS/glycerol-20% before confocal laser scanning examination.

Microgravity Experiments

Microgravity conditions were obtained during a parabolic flight. The flight was performed during the 21st European Spatial Association (ESA) parabolic flight campaign. The 180-min flight consisted of two series of 15 parabolas. Each parabola lasted 3 min and was divided in three different phases of acceleration: 30 sec at 2*g* followed by 25 sec at 0*g* and ending at 30 sec at 2*g*. Five minutes of 1*g* flight separated each group of three parabolas. Control cells were fixed after take-off during a 1*g* period, prior to gravitational stresses. Two experimental groups of cells were fixed after 15 and 30 parabolas.

Confocal Microscopy

The cell preparations were analyzed with a LSM410 confocal scanning laser microscope (Carl Zeiss, Iena, Germany) using a 63x, NA 1.4, Plan-Apochromat oil immersion objective (Carl Zeiss). Vinculin immunofluorescence labeling was imaged in confocal fluorescence microscopy (CFM) and the adhesion plaques were imaged in confocal interferential reflection microscopy (CIRM).

Confocal Fluorescence Imaging. The fluorescence of FITC was excited with the 488 nm line of an air-cooled argon laser. The emission light was separated from the excitation light by a 510 nm dichroic beam splitter. Then a 510-560 nm bandpass filter was used to select the specific fluorescence emission of FITC. One confocal section per cell was recorded with the focus set inside the cell, 0.55 µm from the interface between cell membrane and glass coverslip. Eight images were averaged in order to improve signal-to-noise ratio. The images were coded over a 256 gray level scale.

Confocal Interference Reflection Imaging. The interference reflection images were obtained using the polarized 488 nm line of an air-cooled argon laser. The objective lens was fitted with a Wollaston prism. A rotating polarizer was placed after the confocal pinhole in order to reject internal light reflections from optical parts of the microscope. One confocal section per cell was recorded with the focus set to the level of interface between cell membrane and glass coverslip. This interface was found by changing the focus until the maximum of reflected light was obtained. Eight images were averaged in order to improve signal-to-noise ratio. The images were coded over a 256 gray level scale.

Image Analysis

The confocal images were analyzed using the SAMBA IPS-640 image cytometer (Alcatel-TITN, Grenoble, France). A specific application was written in the proprietary image oriented language of the SAMBA system. The flow chart of this application is given Figure 1. An average of 30 cells per experimental group were analyzed. These cells were measured as they appeared on the slide, with no other selection criterion other than being isolated. Cells in clusters were not measured.

Preprocessing Step. The principal property of confocal imaging is optical slicing. Therefore, it was important that the plane of the glass coverslip was perfectly parallel to the focal plane. A tiny tilt of the glass coverslip creates an intensity gradient in CIRM images. The first step of our program consisted of a background equalization of the gray levels of CIRM images. The principle was to create a virtual image of the background in which the objects (i.e., focal contacts) were wiped out. This was obtained by means of a gray level morphological closing (14,16). Then the gray value of each pixel of the CIRM image was divided by the value of the corresponding pixel of the virtual image of the background (Fig. 2).

Cell Delineation. Neither CIRM images nor CFM images provided continuous information about the cell contours. Therefore, no automatic segmentation scheme could be used to obtain binary masks of the cells. These binary masks were interactively drawn by using the mouse pointer of the SAMBA system.

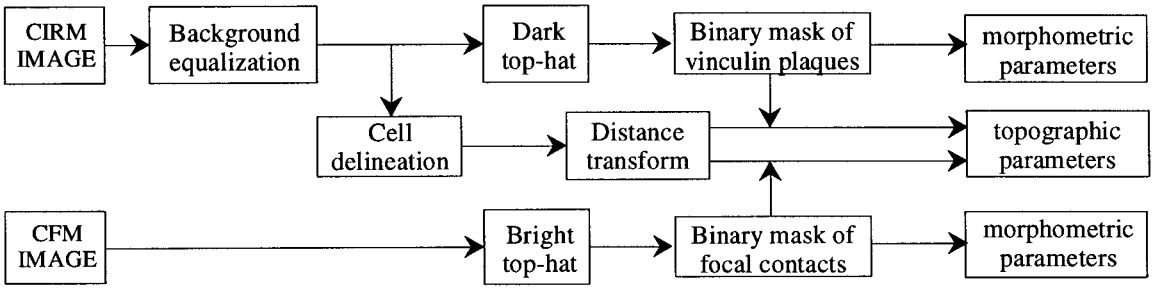

FIG. 1. Diagram of the image analysis program. CIRM: confocal interference reflection microscopy; CFM: confocal fluorescence microscopy.

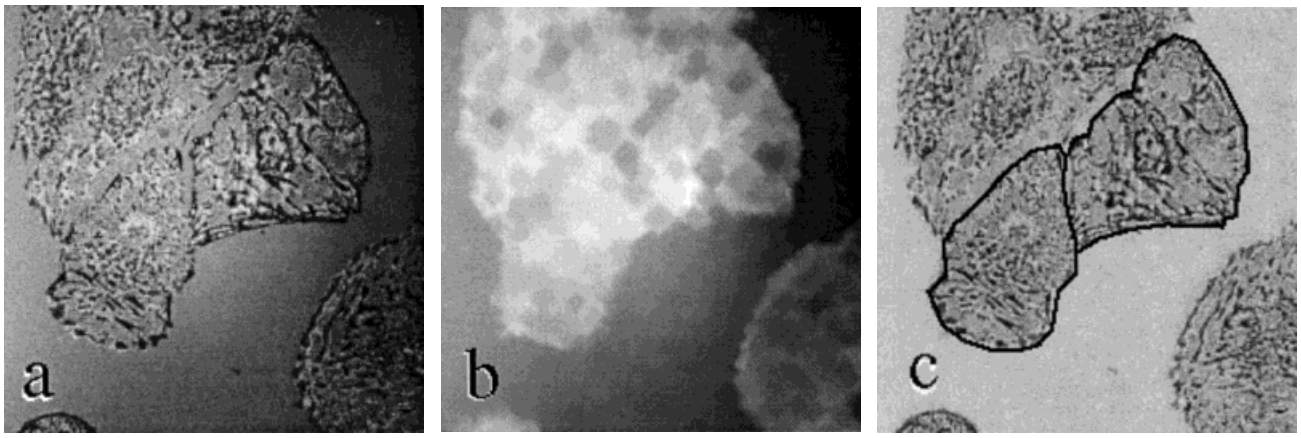

FIG. 2. Background level equalization of confocal interference reflection images. **a**) Raw CIRM image; **b**) morphological closing of the CIRM image; the local gray level minima are wiped out by surrounding brighter gray levels; **c**) corrected image and interactive segmentation; the gray levels of image a are divided pixel by pixel by the gray levels of image b, the contours of the two central cells are shown in black as outlined by the user.

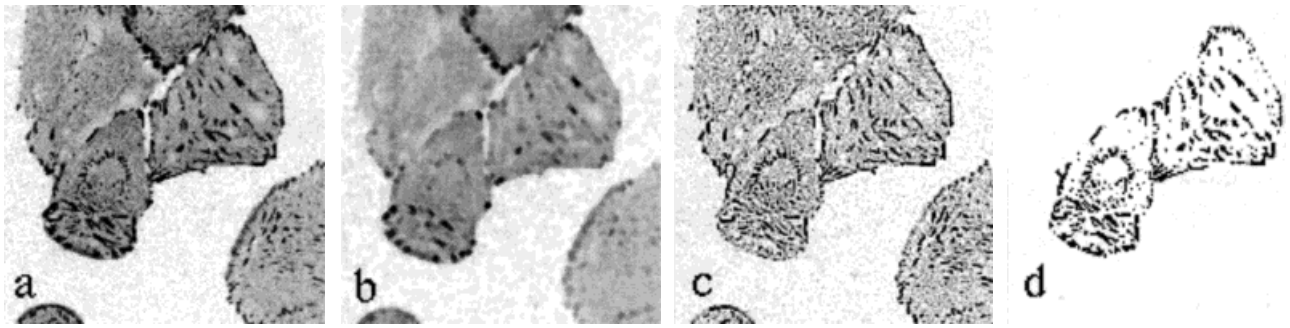

FIG. 3. Segmentation of vinculin spots in confocal fluorescence images. The spot binary image was obtained by means of a top-hat transform. **a**) Confocal fluorescence image; for the sake of readabilty, the fluorescence levels are shown in reverse contrast: high levels (vinculin spots) appear in dark and low levels (background) appear in bright; **b**) morphological open; **c**) image of the differences between a and b; **d**) gray-level thresholding of c; a logical *and* operation with the binary image of cells was applied in order to restrict the measurements to those cells fully contained in the image.

Segmentation of Vinculin Immunofluorescence. The binary masks of vinculin fluorescent spots were obtained by means of a bright top-hat transform (4,11). The top-hat transform is an adaptive thresholding technique (Fig. 3). First we calculated the gray level morphological opening of the CFM image (Fig. 3b). Then the ''open'' image was subtracted from the CFM image (Fig. 3c). Finally, a gray level threshold was applied to the resulting image (Fig. 3d).

Segmentation of Focal Contacts. The binary masks of focal contacts were obtained by means of a dark top-hat transform. The dark top-hat is the same operation as the bright top-hat but with a preliminary inversion of the contrast of CIRM images (i.e., negative image).

Morphological Parameters. Twelve morphological features were calculated by the image analysis program: the area of the cell (CA); the form factor of the cell (i.e.,

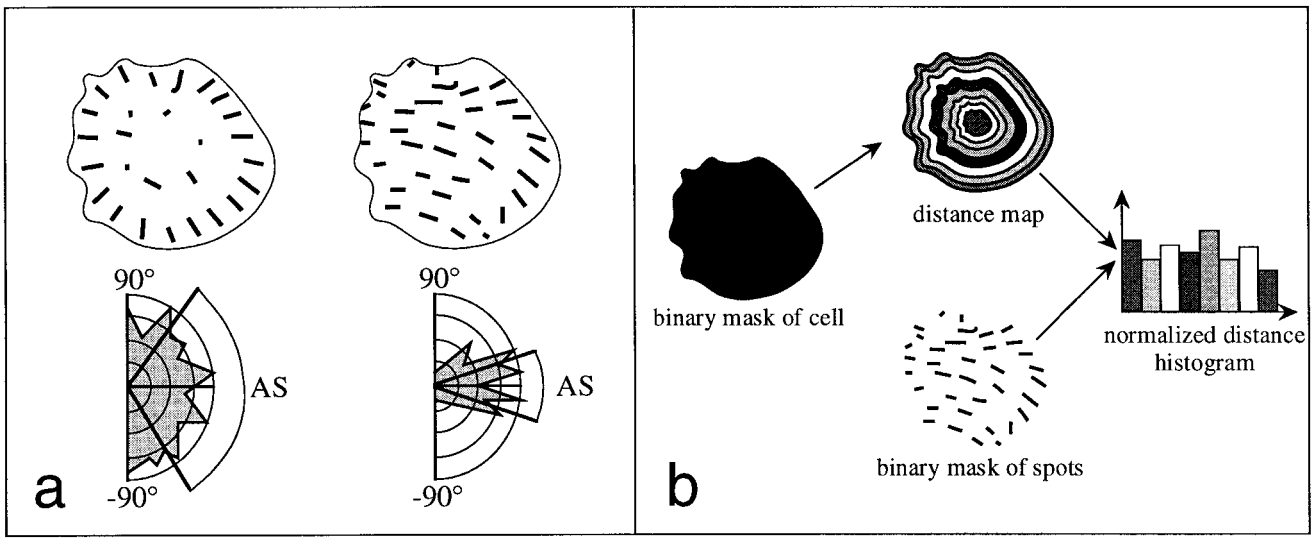

FIG. 4. Calculation of two topographical features. **a**) Angular span: two typical vinculin spot distributions are shown. Left: the spots are mainly distributed in a corona with their greatest axis (length) oriented radially with reference to the center of the cell; the distribution of angles is homogeneous over the -90° to 90° range with a large angular span value. Right: the vinculin spots are regularly aligned along stress lines (association with the cytoskeletton); the distribution of angles is concentrated over a small range. **b**) Average distance from the edge: An isodistance map is calculated from the binary mask of the cell, each layer corresponds to pixels whose distance from the closest edge pixel is the same. A histogram of the distances is calculated by intersecting the distance map and the binary masks of the vinculin spots. Distances are normalized by the greatest distance in the map (i.e., the center of the cell) and the bins are weighted by the corresponding bins of the total histogram of the distance map. The measured feature is the average normalized distance calculated from the weighted histogram.

squared perimeter vs. area) (FF); the ratio of the largest diameter vs. the smallest diameter of the cell (CR); the number of vinculin spots (NVS); the total area of vinculin fluorescence (TVA); the relative area of vinculin fluorescence (RAV); the average area of vinculin spots (AVA) and its standard deviation; the average length of vinculin spots (ALV) and its standard deviation; the average ratio of length vs. width of vinculin spots (RLW) and its standard deviation; and the relative area of focal contact plaques (RAP).

Topographical Parameters. Six topographical features were calculated in order to express the spatial organization of the vinculin spots, as well as their percentage of overlap with focal contacts: the angular span of vinculin spots (AS); the average distance of vinculin spots from the edge of the cell (ADE) and its standard deviation; the area percentage of overlap of vinculin spots and focal contacts (OVF); the area percentage of non-overlapping vinculin spots or isolated vinculin area (IVA); and the area percentage of non-overlapping focal contacts or isolated focal contact area (IFA). Figure 4 illustrates the calculation of AS and ADE. The angular span of vinculin spots (AS, Fig. 4a) was obtained by calculating the standard deviation of the orientation of vinculin spots and expressed the anisotropy of orientation. The average distance from the edge was introduced by Young (20) and used by other authors (15,17) to characterize the average radial distribution of material in a closed shape (Fig. 4b). First the distance map of the binary mask of the cell was built (15) and the histogram of the intersection between the distance map and the binary image of the vinculin spots was calculated. Then the bins of this histogram were weighted by the values of the corresponding bins of the histogram of the total distance map. Finally, ADE was calculated as the average value of the resulting normalized histogram.

Statistical Methods

Multivariate analysis tools were used to compare the experiments and to assess the significance of measurements (or variables). First, all data files were merged and the correlation matrix was calculated. This matrix was examined in order to find redundancies between pairs of features. When a high correlation feature was found, one variable of the pair was discarded from further analysis. This rejected feature was chosen by applying the following rule: either its total correlation (i.e., sum of the absolute values of correlation) with all the remaining features was the greatest, or its biological interpretation was not straightforward.

The experiments were compared by means of stepwise discriminant analysis (SDA). Factorial discriminant analysis (FDA) is a multivariate statistical analysis whose goal is to stress the differences between experimental groups. In other words, the problem addressed was how possible was it to separate experimental groups given measurements on several variables (10). This was achieved by finding linear combinations of variables called ''canonical discriminant functions'' which maximized the variance between groups while minimizing the variance within groups. In order to evaluate the discriminatory role of every variable, FDA was carried out in a stepwise manner. In this case, variables were added to the discriminant

Table 1
Intra- and Interobserver Variations for 12 Features Measured on the Same Set of 10 Cells

Feature	Observer 1	Observer 2	Interobserver
CA	0.53	0.61	0.68
FF	1.24	1.73	0.06
NVS	0.99	1.10	0.24
TVA	1.43	2.10	1.27
PVA	1.08	2.47	0.61
AVA	2.05	2.80	1.04
AS	1.22	1.98	0.20
ADE	**2.89**	3.56	0.30
RAP	0.51	0.53	0.53
OVF	0.33	0.86	0.33
IFA	0.23	0.53	0.24
IVA	2.35	**3.96**	**1.63**

The coefficients of variation are expressed in %. The abbreviations of measurements are given in Materials and Methods. The values shown in boldface correspond to the greatest coefficient of variation in each column.

functions one by one until it was found that adding extra variables did not give significantly better discrimination. The quality of discrimination between each step was assessed by comparing a posteriori probability of group membership of cells with their actual membership. The results were expressed in the form of confusion matrices in which rows correspond to the group of origin and columns correspond to a posteriori group assignment of cells. Ideally, if discrimination was perfect then only the first diagonal of the confusion matrix should be filled with values other than nil. Classification estimates were unbiased; the use of the ''jackknife'' or ''leave-one-out'' procedure ensured that the assignment of a single cell was tested against the a posteriori probabilities involving all the other cells except that cell (10).

The statistical software (correlation analysis and discriminant analysis) was developed in our laboratory in standard C language and is in compliance with the BMDP statistical package.

RESULTS

Assessment of Image Segmentation

Cell delineation and segmentation of focal contacts and vinculin spots was the only part of the program that required human intervention. The operator had to set two gray-level thresholds that were used for all the analyses and had to draw the cell contours. Hence, these were sources of variability of measurement. The intra- and interobserver coefficients of variation were measured on repeated analyses of the same set of cells. The results are given in Table 1. The interobserver coefficients of variation were smaller than 2% and the highest intra-observer variability did not exceed 4%.

Multivariate Analysis

Correlation Analysis. The study of the correlation matrix revealed that eight correlation coefficients were greater than 0.8 in absolute value. The corresponding features were withdrawn from further analysis in order to avoid redundancy. The remaining ten measurements are listed in Table 2.

Table 2
List of the Features Retained for Discriminant Analysis

CA—cell area
FF—cell form factor
CR—ratio of the largest diameter vs. the smallest diameter of the cell
NVS—number of vinculin spots
TVA—total area of vinculin fluorescence
AVA—relative area of vinculin fluorescence
RAP—relative area of focal contact plaques
AS—angular span of vinculin spots
ADE—average distance of vinculin spots from the edge of the cell
IVA—area percentage of non-overlapping vinculin spots or isolated vinculin area

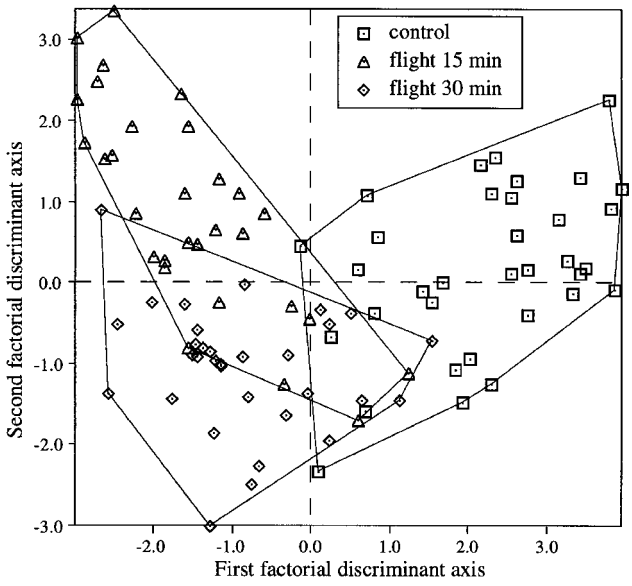

FIG. 5. Factorial discriminant analysis: Projections of the measured cells in the factorial plane. The two axes correspond to the first linear discriminant function and the second linear discriminant function. Control cells (squares); cells fixed after 15 parabolas (triangles); cells fixed after 30 parabolas (diamonds). The convex hulls of the groups are drawn to show the maximum extent of the cell populations.

Discriminant Analysis. Factorial discriminant analysis provided linear combinations of the measured features that described the discriminatory power of the measurements. The maximum number of these linear combinations, also called canonical functions or linear discriminant functions, is equal to the number of cell groups minus one. Thus, a canonical discriminant plane based on the two linear discriminant functions could be built within which the cell measurements were projected (Fig. 5). The extent of the groups and their overlaps were visualized by drawing their convex hulls. The convex hull is the contour of the convex area that encompasses all the points of a set. The first factorial axis mainly separated the control groups from the parabolic flight groups. It appeared that only three control cells were also enclosed within the convex

Table 3
Discriminant Analysis/Confusion Matrix

	Classification		
Group	Control	15 parabolae	30 parabolae
Control (34 cells)	**30** (88%)	1	3
15 parabolae (30 cells)	0	**24** (80%)	6
30 parabolae (32 cells)	0	2	**30** (93%)

Confusion matrix of cell measurements. Total correct classification rate 87.5%. In such a matrix, the rows correspond to the actual experimental group and the columns correspond to the groups to which the cell measurements were assigned on the basis of a posteriori probability. Boldface numbers on the main diagonal indicate the number of well-classified cells; parentheses: the percentage of correct classification for the corresponding row. For example, 30 control cells were correctly re-assigned while four cells could be confused with the two parabolic flight groups.

Table 4
Stepwise Discriminant Analysis: Hierarchy of the Measured Features

Step	Feature	Correct classification
1	CA	66.7%
2	IVA	78.1%
3	CR	80.2%
4	AVA	82.3%
5	RAP	82.3%
6	AS	82.3%
7	FF	87.5%
8	TVA	88.5%
9	ADE	90.6%
10	NVS	87.5%

The abbreviations of feature names are given in Materials and Methods. The step number indicates the introduction of a new variable in the discriminant analysis. For example, at step 4 AVA was added to CA, IVA, and CR. The rate of correct classification (in %) is then calculated in the four-dimensional space defined by these four features.

hulls of the experimental groups. The second factorial axis mainly separated the two experimental groups. Although the convex hulls of the cell populations did overlap, it could be considered that the groups are well discriminated by the measured features. This is confirmed by the analysis of the confusion matrix, listed in Table 3. The rate of correct classification was 87.5%. No cells from the parabolic flight groups were assigned to the control group. Although there was a higher confusion between the experimental groups, the rate of correct classification between the two groups was still high (87%). The stepwise discriminant analysis made it possible to assess the intrinsic discriminatory power of each feature. This yielded to a hierarchy of the measurements, summarized in Table 4. Cell area (CA) was the first parameter to be selected and the confusion matrix for this step showed that this feature primarily separated the control group from the parabolic flight groups. The latter groups were highly confused. The introduction of the measure of isolated vinculin area (IVA) increased dramatically the rate of correct classification from 66.7% to 78.1%. In fact, IVA increased the separation between the 15 parabolas group and the 30 parabolas group. Then CR, AVA, RAP, and AS were introduced but only slightly improved the separation of the three groups. The additions of the cell form factor (FF), the total vinculin area (TVA), and the average distance from edge (ADE) gave the optimal segregation. It must be noted that the number of vinculin spots (NVS) did not improve discrimination.

DISCUSSION

We have developed an approach for the quantitation of focal contact-associated proteins based on a multimodal confocal microscopy and image analysis. It has been applied to the analysis of the distribution of vinculin and focal adhesion in rat osteosarcoma cells submitted to various gravitational stresses. The parts of the program that depended on human intervention did not introduce significant errors in the measured features and only 10 features out of 18 offered independent information. Since the number of cells in each experimental group was significantly greater than the number of measured features, a multivariate analysis was possible. We report here only quantitation of vinculin staining; however, without major changes in procedure the same image analysis could be conducted with other focal contact-associated proteins, such as Talin and Paxillin, or other proteins which co-localize with vinculin, such as phosphotyrosine (PY-20).

Stepwise discriminant analysis showed that significant differences existed between control cells and cells submitted to parabolic flights. In fact, few cells were confused between the two groups. The changes induced by the mechanical stresses affected mainly the morphometrical features: cell area, cell shape, and size of vinculin spots. However, the number of vinculin spots was not found to improve discrimination, although this feature showed significant differences between groups when a classical Student's t-test was used. In fact, NVA appeared to be highly correlated with two other features included in the analysis: CR ($r = 0.74$) and TVA ($r = 0.75$). This is why this variable was included only in last position. Another interesting point is that IVA was included in the second step. IVA expressed the area of isolated vinculin spots, that is, those that did not overlap with the physical focal contacts. This suggested that the mechanical stresses induced modifications of the relative distribution of vinculin and focal contacts.

The results presented in this paper are preliminary and are given to present the confocal image analysis method. They must be confirmed by a more complete and detailed analysis. In particular, the number of cells studied here is very small: around 30 cells per group. However, since no selection scheme other than measuring isolated cells was used, we may expect that our samples are not too biased. A larger number of cells (>100) per group and an independent test set must be used to confirm the results. In order to interpret the modifications of cell shape and of the relative distribution of vinculin and focal contacts, it is necessary to add more experimental conditions. Indeed, there was an alternance of $2g$ and $0g$ acceleration periods during the parabolic flights, and it is difficult to distinguish

their respective importance. Therefore, this study must be completed by measuring the same features in cell populations that were submitted to a constant 2*g* acceleration or submitted to simulated 0*g* acceleration in a clinostat (1) or real microgravity (orbital space flight). Such additional experiments are currently being undertaken.

LITERATURE CITED

1. Briegleb W: Some quantitative aspects of the fast-rotating clinostat as a research tool. ASGSB Bulletin 5:23–30, 1992.
2. Ben Ze'ev A, Reiss R, Bendori R, Gorodecki B: Transient induction of vinculin gene expression in 3T3 fibroblats stimulated by serum growth factors. Cell Regul 1:621–636, 1990.
3. Carvalho RS, Scott JE, Suga DM, Yen EH: Stimulation of signal transduction pathways in osteoblast by mechanical strain potentiated by parathyroid hormone. J Bone Miner Res 9:999–1011, 1994.
4. Cornelisse CJ, van Driel-Kulker AM, Meyer F, Ploem JS: Automated recognition of atypical nuclei in breast cancer cytology specimens by iterative image transformations. J Microsc 137:101–110, 1985.
5. Deroanne CF, Colige AC, Nusgens BV, Lapiere CM: Modulation of expression and assembly of vinculin during in vitro fibrillar collagen-induced angiogenesis and its reversal. Exp Cell Res 224:215–223, 1996.
6. Guignandon A, Vico L, Alexandre C, Lafage-Proust MH: Shape changes of osteoblastic cells under gravitational variations during parabolic flight: Relationship with PGE2 synthesis. Cell Struct Funct 20:369–375, 1995.
7. Jones DB, Leivseth G, Goodship A, Sasse L, Van der Sloten J: Osteoblast intracellular free calcium measurements in microgravity by ratio imaging and photometry. In: Experiment Results of ESA and CNES Parabolic Flight Campaigns 10th Anniversary of First ESA Parabolic Flight Campaign. European Spatial Agency (ed). ESA WPP 90:363–380, 1995.
8. Jones DB, Brockmann E, Sasse L, Van der Sloten J, Goodship A, Leivseth G, Tenbosch J: Real time investigation of mechano-tranduction in osteoblasts during parabolic-flight. Low G 7:14–17, 1996.
9. Kubota T, Yamauchi M, Onozaki J, Sato S, Suzuki Y, Sodek J: Influence of an intermittent compressive force on matrix protein expression by ROS 17/2.8 cells, with selective stimulation of osteopontin. Arch Oral Biol 38:23–31, 1993.
10. Manly BFJ: Discriminant function analysis. In: Multivariate Statistical Methods. A Primer. London, New York: Chapman and Hall, 1986, pp 86–99.
11. Meyer F: Image analysis: A consumer's guide. Microsc Acta Suppl 6:61–68, 1983.
12. Miyamoto S, Teramoto H, Coso O, Gutking J, Burbelo P, Akiyama S, Yamada K: Integrin function: Molecular hierarchies of cytoskeletal and signaling molecules. J Cell Biol 131:791–805.
13. Rodan GA: Perspectives: Mechanical loading, estrogen deficiency and the coupling of bone formation to bone formation. J Bone Miner Res 6:527–530, 1991.
14. Russ JC: Computer Assisted Microscopy: The Measurement and Analysis of Images. New York: Plenum Press, 1990.
15. Russ JC, Russ JC: Uses of the euclidian distance map for the measurement of features in the images. J Comp Assist Microsc 1:343–375, 1989.
16. Serra J: Image Analysis and Mathematical Morphology. Academic Press, London, 1982.
17. Usson Y, Humbert C: Methods for topographical analysis of intra-nuclear BrdUrd-tagged fluorescence, Cytometry 13:595–602, 1992.
18. Wang N, Ingber DE: Control of cytoskeletal mechanics by extracellular matrix, cell shape, and mechanical tension. Biophys J 66:2181–2189, 1994.
19. Wood CK, Turner CE, Jackson P, Critchley DR: Characterisation of the paxillin-binding site and C terminal focal adhesion targeting sequence in vinculin. J Cell Sci 107:709–717, 1994.
20. Young IT, Verbeek PW, Mayall BH: Characterization of chromatin distribution in cell nuclei. Cytometry 7:467–474, 1986.